

Vertical nanowire electrode arrays as a scalable platform for intracellular interfacing to neuronal circuits

Jacob T. Robinson^{1‡}, Marsela Jorgolli^{2‡}, Alex K. Shalek¹, Myung-Han Yoon^{1†}, Rona S. Gertner¹ and Hongkun Park^{1,2*}

Deciphering the neuronal code—the rules by which neuronal circuits store and process information—is a major scientific challenge^{1,2}. Currently, these efforts are impeded by a lack of experimental tools that are sensitive enough to quantify the strength of individual synaptic connections and also scalable enough to simultaneously measure and control a large number of mammalian neurons with single-cell resolution^{3,4}. Here, we report a scalable intracellular electrode platform based on vertical nanowires that allows parallel electrical interfacing to multiple mammalian neurons. Specifically, we show that our vertical nanowire electrode arrays can intracellularly record and stimulate neuronal activity in dissociated cultures of rat cortical neurons and can also be used to map multiple individual synaptic connections. The scalability of this platform, combined with its compatibility with silicon nanofabrication techniques, provides a clear path towards simultaneous, high-fidelity interfacing with hundreds of individual neurons.

So far, most microfabricated neuronal interfaces have been based on electrodes that reside outside the cellular membrane, which prevents them from being used to measure sub-threshold events and also prohibits precise cell-to-electrode registration^{3,5–12}. Recently, emerging nanofabrication techniques have enabled the development of new micro- and nanoscale devices that exhibit significantly improved electrical coupling between cells and electrodes. Notably, gold mushroom-shaped microelectrodes have been used to perform ‘intracellular-like’ recordings from *Aplysia* neurons and mammalian cell lines^{13,14}, and true intracellular recordings from several mammalian cell lines and cardiomyocytes have been realized using microfabricated planar patch-clamp devices^{15–17} and kinked nanowire probes¹⁸. Although these examples represent major advances in cell–electrode coupling, either they have been too large to interface with mammalian neurons^{13–17} or they lack the scalability required to perform simultaneous measurements of multiple cells¹⁸.

Our vertical nanowire electrode array (VNEA) was specifically designed to address these issues by making use of the same nanofabrication technology that enables mass production of integrated silicon electronic circuits. Figure 1 presents a prototype VNEA with 16 stimulation/recording pads. The entire device was fabricated from a silicon-on-insulator (SOI) substrate so that each pad could be independently addressed electrically (see Methods and Supplementary Fig. S1 for additional fabrication details). At the centre of each stimulation/recording pad lies a 3×3 array of nine silicon nanowires (diameter, ~ 150 nm; length, $3 \mu\text{m}$; pitch, $2 \mu\text{m}$). Each nanowire in the array consists of a degenerately doped silicon core encapsulated by a silicon dioxide (glass) shell,

and is capped with a sputter-deposited metal tip (titanium/gold; Fig. 1a). The silicon core and metal tip provide electrical access to the interior of the cell, and the glass shell plays the dual role of preventing current leakage through the nanowire sidewalls and serving as a material with which to make tight seals to the cell membrane⁴. The geometry of each nanowire array (a $4 \mu\text{m}$ square) was chosen to be smaller than the size of a typical neuronal cell body so as to increase the probability of single-neuron coupling.

The top-down nanofabrication technology used here enables precise control over the physical dimensions of the nanowires, as well as the size and configuration of the stimulation/recording pads. Moreover, the number of pads could be scaled up to thousands. Because of its planar integrated geometry, the VNEA is well suited to studying *in vitro* dissociated neuronal circuits and quasi-two-dimensional *ex vivo* preparations, such as brain slices or retina. It can also be readily coupled with fluorescence microscopy^{19,20}, optogenetic techniques²¹ and conventional patch measurements⁴, allowing truly multiplexed interrogation of neuronal circuits. As an example, Fig. 1f shows a typical network of dissociated rat cortical neurons on top of a VNEA after five days *in vitro* (DIV). Images obtained by means of confocal microscopy demonstrate that the neurons sitting directly on top of the nanowires envelop them and, at times, appear penetrated (Fig. 1e, Supplementary Fig. S2). Meanwhile, whole-cell patch-clamp measurements show that neurons cultured on the VNEAs have similar electrophysiological characteristics as those cultured on glass coverslips, as previously observed²².

We optimized the operation protocols for our VNEA devices using HEK293 cells as a model system. HEK293 cells are advantageous for establishing stimulation and recording procedures because they require a short culture time before electrical interrogation (only a few hours), and their membrane resistance remains constant within 15 mV of the resting membrane potential²³. To determine the device parameters that characterize the VNEA/cell interface, we performed whole-cell patch-clamp recordings of HEK293 cells residing directly on top of the nanowires and monitored voltages and currents simultaneously using both a patch pipette and a VNEA pad (Fig. 2a). In more than half of the cases, the membrane potential changed immediately upon VNEA current injection, suggesting that the nanowires had spontaneously penetrated the cell membrane. When the membrane potential of a cell did not change significantly upon current injection (that is, when the nanowires were not inside the cell), we used a short voltage pulse ($\sim \pm 3$ V; duration, 100 ms) to permeabilize the cell membrane²⁴ and promote nanowire penetration (see Methods).

¹Department of Chemistry and Chemical Biology, Harvard University, Cambridge, Massachusetts 02138, USA, ²Department of Physics, Harvard University, Cambridge, Massachusetts 02138, USA; [†]Present address: School of Materials Science and Engineering, GIST, Republic of Korea; [‡]These authors contributed equally to this work. *e-mail: Hongkun_Park@harvard.edu

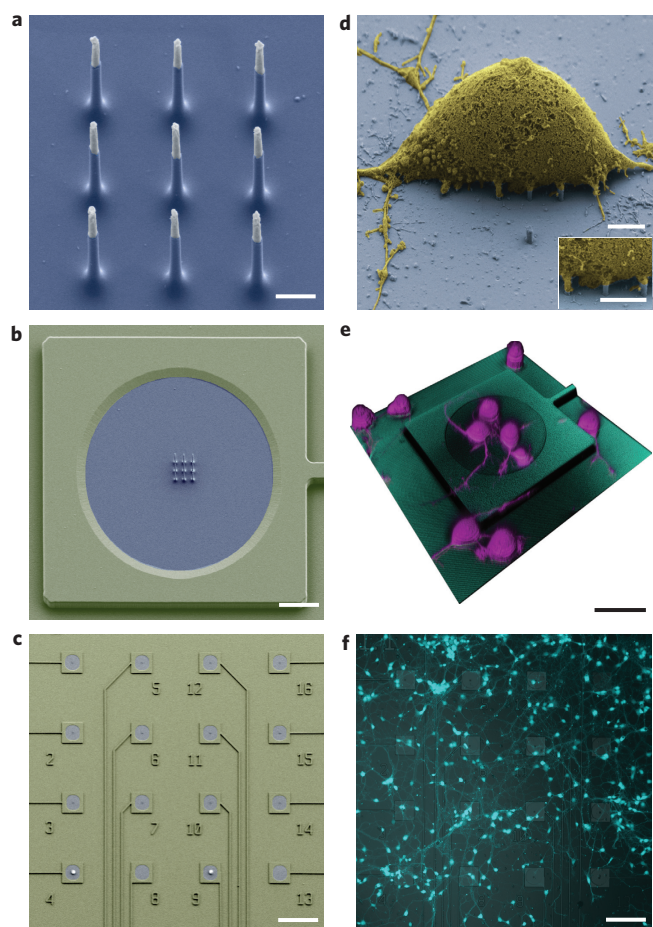


Figure 1 | VNEA for interrogating neuronal networks. **a**, SEM image of the nine silicon nanowires that constitute the active region of a VNEA. Dimensions of the nanowire electrodes were designed to facilitate single-cell intracellular electrical coupling. False colouring shows metal-coated tips (grey) and insulating silicon oxide (blue). Scale bar, 1 μm . **b**, SEM image of a VNEA pad. False colouring indicates additional insulation from Al_2O_3 (green). Scale bar, 10 μm . **c**, SEM image of a device consisting of 16 stimulation/recording pads for parallel multi-site interrogation of neuronal circuits. Scale bar, 120 μm . **d**, SEM image of a rat cortical cell (3 DIV, false-coloured yellow) on top of a VNEA pad (false-coloured blue; scale bar, 2.5 μm), showing nanowires interfacing with the cellular membrane (inset; scale bar, 2.5 μm). **e**, Reconstructed three-dimensional confocal microscope image of rat cortical neurons cultured on a VNEA pad (3 DIV). Scale bar, 40 μm . **f**, Representative optical microscope image of calcein AM-labelled rat cortical neurons (cyan) cultured on a VNEA (5 DIV). Scale bar, 120 μm .

Once the nanowires had access to the interior of the cell, the VNEA device was used to measure and control the cell's membrane potential (V_m) by taking advantage of the electrochemistry at the nanowire tips. Specifically, when no voltage was applied to the nanowires, the change in V_m induced by the patch pipette led to a change in the nanowire voltage (V_{NW}) due to the charging/discharging of the electrical double layer at the metal-coated nanowire tips (the 'capacitive' regime; Fig. 2b, left column). Changes in V_m could also be recorded by applying a bias ($\sim -1.5\text{ V}$) to the nanowires that was sufficient to flow a small electrochemical current; in this 'Faradaic' regime, the value of V_{NW} required to maintain a fixed current tracked the changes in V_m , in a fashion similar to conventional current-clamp techniques⁴ (Fig. 2b, centre column). Finally, when current was injected through the nanowires, the voltage measured at the patch pipette (V_p) changed (Fig. 2b, right panel, and Supplementary Fig. 3), indicating that nanowire-based

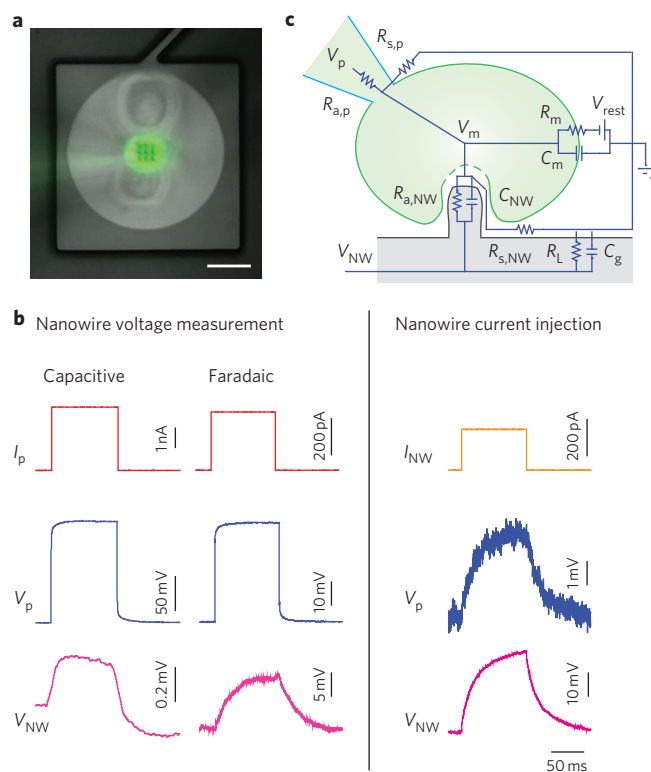


Figure 2 | Characterization of the VNEA/cell electrical interface. **a**, Composite bright-field and fluorescence image of a patched HEK293 cell on a VNEA pad (0 DIV). Calcein (green) was added to the intracellular recording solution to enable fluorescence imaging of the patched cell. Scale bar, 20 μm . **b**, Current injected into the pipette (I_p) versus time in capacitive and Faradaic modes (top row, left and middle columns, respectively), and the resulting voltage response of the cell recorded with a patch pipette V_p (middle row) and a VNEA pad V_{NW} (bottom row). Patch-pipette recordings confirm that the membrane potential of the cell can be controlled by injecting a current I_{NW} (right column). Note that capacitive and Faradaic measurements were performed on different cells because switching between recording modes required swapping the amplifier electronics. **c**, Equivalent-circuit model of the VNEA/cell interface. $R_{\text{a,NW}}$, $R_{\text{s,NW}}$, $R_{\text{a,p}}$ and $R_{\text{s,p}}$ represent the access and seal resistances for the nanowires and pipettes. The capacitance of the electrical double layer at the nanowire surface is represented as C_{NW} . The equivalent circuit also includes the leak resistance due to uncoupled nanowires or defects in the electrode insulation (R_L) and the parasitic capacitance due to the device and associated electronics (C_g). The cell itself has a characteristic membrane resistance (R_m), capacitance (C_m) and resting potential (V_{rest}), all of which combine to determine the potential across the cell membrane (V_m). The values of these circuit elements were determined based on simultaneous patch pipette and VNEA measurements such as those shown in **b**.

control over the membrane potential is also possible (note that because the nanowires provide only a small point source of current, changes to the membrane potential may not be uniform throughout the cell). In the Faradaic regime, when current was injected through the pipette, voltage changes measured at the nanowire were ~ 3 times smaller than those measured at the pipette. On the other hand, when current was injected through the nanowire, voltage changes measured at the pipette were ~ 10 times smaller than those measured at the nanowire. In the capacitive regime, V_{NW} was ~ 300 times smaller than V_p .

During capacitively coupled measurements, V_p typically rose by $\sim 10\text{ mV}$ from the initial resting potential after 30 min of recording. Such a rise was common even for patch pipette recordings without

nanowire penetration, suggesting that the duration of our measurement was limited not by the nanowire recording but rather by effects from patching. During capacitive measurements, a reduction in the signal amplitude measured at the nanowires was also observed over the course of a few minutes, indicating partial recovery of the permeabilized membrane. However, this signal could be repeatedly restored to full strength by reapplying the permeabilization protocol. In the Faradaic regime, no signal reduction was observed, probably owing to the constant current flow at the nanowire tips. It should be noted that, unlike capacitive measurements, the continuous recording time in the Faradaic regime was typically limited to less than 10 min, most probably owing to prolonged electrochemical reactions damaging the cellular membrane. By performing measurements intermittently, however, the interrogation period could be extended significantly.

Analysis of the current–voltage traces measured at the patch pipette and the nanowire (Fig. 2b, Supplementary Fig. S4) using the equivalent circuit model in Fig. 2c enabled the determination of all of the parameters that specify the electrical coupling between the cell and the nanowires (see Supplementary Information for details). In particular, this analysis showed that the seal resistance ($R_{s,NW}$) between the nanowires and the cell membrane ranged between 100 and 500 M Ω , and the total double-layer capacitance at the nanowire tips (C_{NW}) (ref. 25) was typically ~ 1 pF. The nanowire access resistance ($R_{a,NW}$), which includes the intrinsic nanowire resistance and the resistance at the electrochemical junction and thus varies with V_{NW} , was determined to be infinite at zero bias (no electrochemical reactions occur at the metal tips) and ~ 300 M Ω at $V_{NW} \approx -1.5$ V. When the measurement was performed in the Faradaic regime, this large $R_{a,NW}$, combined with the parasitic capacitance to ground (C_g) of a typical VNEA pad and its associated electronics (~ 150 pF), resulted in an RC time constant on the order of 10 ms. Although this RC component filtered the voltage waveform measured at the nanowires (compared to that measured at a patch pipette), this distortion could be easily corrected using a deconvolution procedure (see Supplementary Information and Fig. S5). In the capacitive regime, the change in V_{NW} originated from the charging and discharging of the electrical double layer and thus accurately followed fast changes in V_m . The magnitude of this response, however, was attenuated due to capacitive voltage division ($\sim C_{NW}/C_g$).

Once the device characterization and protocol optimization were complete, we used the VNEA to perform high-fidelity intracellular stimulation and recording of rat cortical neurons (Fig. 3, Supplementary Fig. S6). Typically, these neurons were interrogated after 6–14 DIV to allow electrophysiological development and the formation of synaptic connections^{26,27}. As shown in Fig. 3c and Supplementary Fig. 6, current pulses injected into neurons via the nanowires reliably evoked neuronal action potentials (APs), as recorded by means of simultaneous whole-cell patch clamp. The stimulation probability followed a sigmoidal dependence on the magnitude of the nanowire-injected current (Fig. 3b), similar to that reported for patch pipette stimulation²⁸. Moreover, the VNEA operating in current-clamp mode could be used to monitor individual APs evoked by the patch pipette. For single-shot AP measurements, the signal-to-noise ratio for VNEA recordings was typically 100 or greater (Fig. 3d). When we averaged multiple waveforms obtained under identical experimental conditions, we could improve the signal-to-noise ratio to $>1,000$ (Supplementary Fig. S5). This suggests that by averaging the response to repeated presynaptic stimulations, postsynaptic potentials (PSPs) could be measured using the VNEA.

The multiplexed stimulation and recording capabilities of the VNEA platform and its compatibility with conventional patch-clamp and fluorescence microscopy techniques enable comprehensive examination of the functional connectivity in neuronal circuits beyond

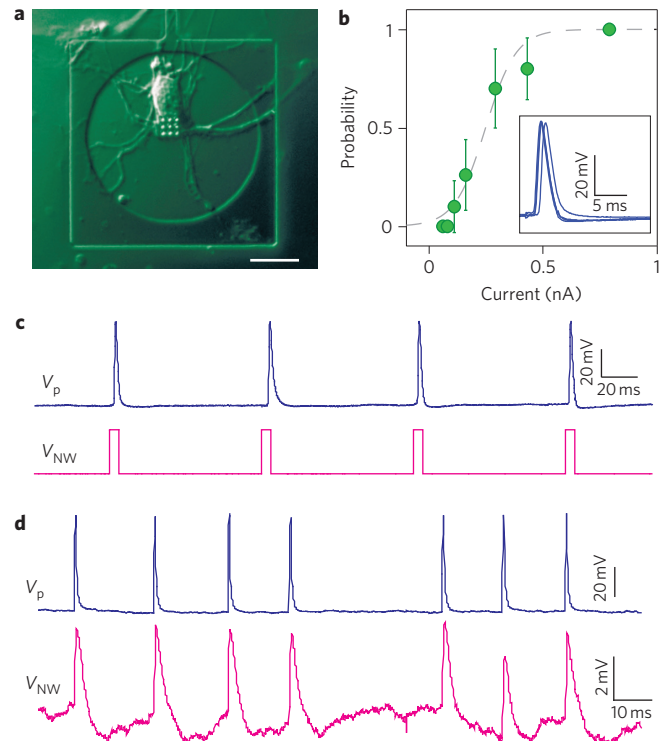


Figure 3 | Stimulation and recording of rat cortical neurons using a VNEA. **a**, Representative DIC micrograph of a rat cortical neuron cultured on a VNEA pad (6 DIV). Scale bar, 20 μm . **b**, Probability of AP excitation plotted as a function of current injected by nanowires shows a sigmoidal dependence (dashed line), which is similar to AP excitation elicited by intracellular patch pipettes. Probabilities were calculated for 20 trials and plotted as a function of the stimulation current. Error bars represent 95% confidence intervals. Inset: five consecutive time-aligned action potentials stimulated by nanowire current injection show less than 1 ms jitter. **c**, APs were reliably stimulated by voltage pulses V_{NW} at the VNEA pad (magenta) and recorded using a patch pipette (blue). **d**, Similarly, action potentials were stimulated using a patch pipette (blue) and recorded by the VNEA pad in Faradaic mode (magenta). VNEA measurements show good agreement with those obtained simultaneously by a patch pipette.

traditional connected-pair studies²⁹. To illustrate the potential of such measurements, we used our VNEA platform to map multiple individual synaptic connections onto a single postsynaptic neuron. Specifically, we used a patch pipette to measure the PSPs of a single neuron in a dissociated neuronal culture while inducing APs in other neurons using neighbouring VNEA pads (Fig. 4a). By monitoring PSP responses following repeated stimulations at each pad, we found that excitation of some of the nearby neurons reproducibly generated either excitatory (EPSPs) or inhibitory PSPs (IPSPs) in the patch-clamped cell (Fig. 4b,c). The latency window of these EPSPs and IPSPs ranged from 2 to 8 ms, indicative of a monosynaptic connection³⁰. We note that performing this type of measurements using conventional patch-clamp techniques would require each presynaptic cell to be individually identified and patched separately. Using our VNEA platform, this process can be significantly simplified and expedited. Together, the magnitude, sign and latency of these PSPs define the functional connectivity of a neuronal circuit. By monitoring changes in this connectivity as a function of time and combining it with structural reconstruction techniques, we should be able to investigate the relationships among the architecture, dynamics and function of neuronal circuits in unprecedented detail.

The present study demonstrates that the VNEA platform can be used to stimulate and record neuronal activities in a scalable fashion.

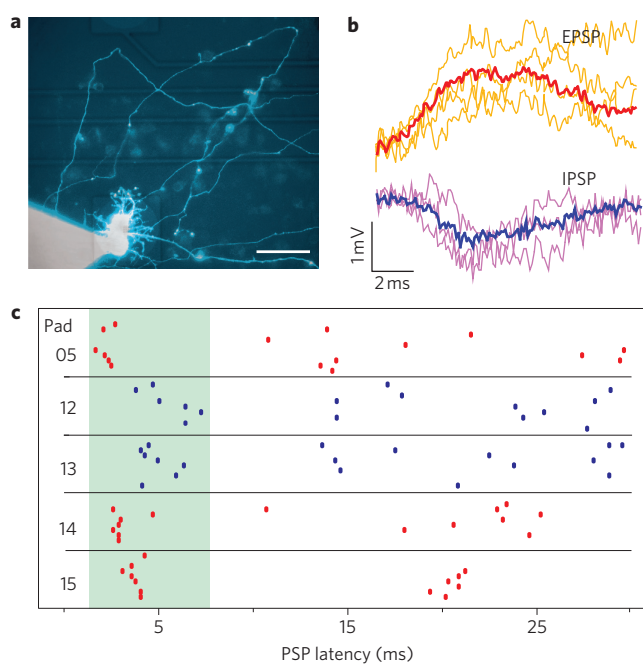


Figure 4 | Identification of functional synaptic connectivity using a VNEA and a patch pipette. **a**, Composite bright-field and fluorescence image of a cortical neuron patched and backfilled with calcein (14 DIV). Scale bar, 35 μm . **b**, Representative EPSPs (top) and IPSPs (bottom) were averaged (bold) and used as templates for identifying other PSPs recorded using a patch pipette. To measure these PSP events, we injected a constant current through the patch pipette to hold the membrane potential near -40 mV. At this resting potential, EPSPs and IPSPs produce positive or negative changes in the membrane potential, respectively, allowing them to be distinguished from one another. **c**, Raster plots of EPSPs (red) and IPSPs (blue) identified by patch-clamp recording and plotted as a function of their latency following stimulation at the specified VNEA pads. Each of the five pads shown here evoked reproducible PSPs in the patched cell within a latency window of 2–8 ms (green), suggesting monosynaptic connectivity.

Moreover, the VNEA platform can be readily coupled with conventional patch measurements, fluorescence microscopy and optogenetic techniques, allowing multiplexed interrogation of a neuronal circuit. Although the prototype demonstrated here has only 16 stimulation/recording sites, higher numbers and densities can readily be achieved using standard silicon nanofabrication processes. For instance, contemporary deep UV lithography with feature sizes near 150 nm can produce recording pad densities approaching 10,000 electrodes mm^{-2} . The integration of complementary metal-oxide-semiconductor circuitry with a VNEA would further allow on-chip digitization, signal multiplexing, compression and telemetry. Finally, the small dimensions and planar geometry of VNEAs should facilitate their incorporation into implantable electrodes, similar to the silicon-based microelectrode array implants currently in use³¹, opening up new possibilities for neuronal prosthetics and large-scale studies of neuronal circuit dynamics *in vivo*.

Methods

Device fabrication. Nanowires on the VNEA devices were fabricated using electron-beam lithography followed by reactive ion etching and thermal oxide thinning. Nanowire tips were metal-coated by means of thermal or electron-beam evaporation. Electrode tracks were defined using photolithography and reactive ion etching followed by atomic layer deposition of an aluminium oxide layer to provide electrical isolation from the culture media (see Supplementary Information for more details).

Cell culture and imaging. Cells and cell culture media were contained within polydimethylsiloxane wells bonded to the VNEA surface (see Supplementary Information for details). Epifluorescence and differential interference contrast (DIC)

images of live cells were overlaid and coloured using ImageJ. False colouring of scanning electron microscopy (SEM) images was performed using Photoshop CS3 (Adobe).

Membrane permeabilization and visualization. Typically, the membrane potential, as measured using a patch pipette, responded immediately to the application of current via the VNEA pad (-200 to -400 pA), suggesting that some of the nanowires formed a tight seal with the cell membrane and penetrated the cell on top. In the absence of immediate electrical coupling, permeabilization could be achieved by applying 100 ms voltage pulses with amplitudes of $\sim\pm 3$ V. Membrane permeabilization was typically accompanied by a depolarization of V_m by ~ 10 – 20 mV, and lowering the holding current on the recording pad or the patch pipette reversed this depolarization. Confocal microscopy imaging of cortical neurons cultured on vertical silicon nanowires (3 DIV) showed that some neurons appeared penetrated by nanowires while others did not, consistent with our electrical measurements (Supplementary Fig. S3). Images were obtained by labelling the nanowires with Alexa647-SE in dimethylsulphoxide (DMSO; 1 mg ml^{-1} , Invitrogen)²². After incubation for 30 min at 37 °C, samples were washed three times through water, blown dry and used as a substrate for neuron culture. Before imaging, neuronal membranes were labelled by incubating the samples in an extracellular solution containing 1:100 Vybrant DiI (Invitrogen) at room temperature. Images were then analysed and reconstructed in three dimensions using Imaris 6.2 (Bitplane).

Patch pipette recording. During measurements, VNEA substrates were bathed in a solution containing NaCl (119 mM), KCl (5 mM), HEPES (20 mM), CaCl_2 (2 mM), MgCl_2 (2 mM), glucose (30 mM) and glycine (0.001 mM). The pH of the solution was 7.3 and the osmolarity was 330 mosM (adjusted with sucrose). Patch pipettes were pulled to have resistances of ~ 2 – 10 M Ω and then backfilled with a solution containing potassium gluconate (130 mM), KCl (10 mM), MgCl_2 (5 mM), EGTA (0.6 mM), HEPES (5 mM), CaCl_2 (0.06 mM), Mg-ATP (2 mM), GTP (0.2 mM), leupeptine (0.2 mM), phosphocreatine (20 mM) and creatine phosphokinase (50 U ml^{-1}) at pH 7.2 (ref. 32). For certain experiments, high-purity calcein (Invitrogen) was added (1 part in 5,000) to the intracellular recording solution to enable fluorescence imaging of the patched cell. All recordings were made at room temperature with a Multiclamp 700B (Molecular Devices). Current-clamp recordings of HEK293 cells were performed with a holding current of 0 pA. During neuronal measurements, the holding current was adjusted to bring the neuron to a resting membrane potential near -70 mV for stimulation and recording experiments, and -40 mV for PSP identification. The pipette capacitance was corrected electronically. All acquisitions were performed using the pCLAMP 10 software (Molecular Devices) and analysed and plotted using Clampfit 10 (Molecular Devices) and Matlab (Mathworks).

Protocols for VNEA stimulation and recording. The devices were mounted in a custom-built aluminium enclosure designed to provide both electrical connection to the VNEA pads and electromagnetic shielding. The connection between the VNEA and stimulation/measurement electronics was achieved using conductive elastomeric connectors (ZEBRA, Fuji-poly) and a custom-built printed circuit board. Neuronal stimulation was achieved using a 32-channel analogue output module (National Instruments PXI-6723) and control software written in LabView (National Instruments). During VNEA stimulation, capacitive electronic crosstalk between the patch pipette and VNEA was removed by subtracting the characteristic transients. Current-clamp measurements were performed using a custom-built current-clamp circuit with stability on the order of 10 pA and compliance values between ± 10 V and ± 5 nA. Currents were controlled using our analogue output module, and recorded voltages were amplified using AM Systems Model 1800 (gain, $\times 100$; bandwidth, 1 Hz–20 kHz). Both pre- and post-amplified voltages were collected and digitized. Capacitively coupled measurements were recorded directly with the AM Systems amplifier, and digitally filtered to remove 120 Hz line noise. To preserve the simultaneity of the pipette and VNEA measurements, all signals were recorded and digitized simultaneously using the pCLAMP 10 software and a 16-channel analogue data acquisition system (Axon Digidata 1322A, Molecular Devices). Steady-state control of the membrane potential (as measured by the patch pipette, V_p) could be achieved for several seconds by changing the offset voltage applied to the nanowires (V_{NW}) (Supplementary Fig. S3).

PSP identification. To identify EPSPs and IPSPs, we patched a rat cortical neuron (14 DIV) in whole-cell current-clamp mode. Several representative EPSPs/IPSPs were manually identified and averaged to form a template (Fig. 4b). Once a template was obtained, automatic event detection was performed using Clampfit 10. Latencies were calculated as the interval between the rising edge of the stimulus and the peak of the PSP. Data were then compiled and plotted using Matlab.

Received 9 November 2011; accepted 7 December 2011;
published online 10 January 2012

References

1. Yuste, R. Circuit neuroscience: the road ahead. *Front. Neurosci.* **2**, 6–9 (2008).
2. Bock, D. D. *et al.* Network anatomy and *in vivo* physiology of visual cortical neurons. *Nature* **471**, 177–182 (2011).

3. Pine, J. A history of MEA development, in *Advances in Network Electrophysiology* (eds, Taketani, M. & Baudry, M.) 3–23 (Springer, 2006).
4. Molleman, A. *Patch Clamping* (Wiley, 2003).
5. Rolston, J. D., Gross, R. E. & Potter, S. M. A low-cost multielectrode system for data acquisition enabling real-time closed-loop processing with rapid recovery from stimulation artifacts. *Front. Neuroeng.* **2**, 12–12 (2009).
6. Voelker, M. & Fromherz, P. Signal transmission from individual mammalian nerve cell to field-effect transistor. *Small* **1**, 206–210 (2005).
7. Kim, D-H. *et al.* Dissolvable films of silk fibroin for ultrathin conformal bio-integrated electronics. *Nature Mater.* **9**, 511–517 (2010).
8. Viventi, J. *et al.* A conformal, bio-interfaced class of silicon electronics for mapping cardiac electrophysiology. *Sci. Trans. Med.* **2**, 24ra22 (2010).
9. Patolsky, F. *et al.* Detection, stimulation, and inhibition of neuronal signals with high-density nanowire transistor arrays. *Science* **313**, 1100–1104 (2006).
10. Eschermann, J. F. *et al.* Action potentials of HL-1 cells recorded with silicon nanowire transistors. *Appl. Phys. Lett.* **95**, 083703 (2009).
11. Wang, K., Fishman, H. A., Dai, H. & Harris, J. S. Neural stimulation with a carbon nanotube microelectrode array. *Nano Lett.* **6**, 2043–2048 (2006).
12. McKnight, T. E. *et al.* Resident neuroelectrochemical interfacing using carbon nanofiber arrays. *J. Phys. Chem. B* **110**, 15317–15327 (2006).
13. Hai, A. *et al.* Spine-shaped gold protrusions improve the adherence and electrical coupling of neurons with the surface of micro-electronic devices. *J. R. Soc. Interface* **6**, 1153–1165 (2009).
14. Hai, A., Shappir, J. & Spira, M. E. In-cell recordings by extracellular microelectrodes. *Nature Methods* **7**, 200–202 (2010).
15. Lau, A. Y., Hung, P. J., Wu, A. R. & Lee, L. P. Open-access microfluidic patch-clamp array with raised lateral cell trapping sites. *Lab Chip* **6**, 1510–1515 (2006).
16. Li, X., Klemic, K. G., Reed, M. A. & Sigworth, F. J. Microfluidic system for planar patch clamp electrode arrays. *Nano Lett.* **6**, 815–819 (2006).
17. Sigworth, F. J. & Klemic, K. G. Microchip technology in ion-channel research. *IEEE Trans. Nanobiosci.* **4**, 121–127 (2005).
18. Tian, B. *et al.* Three-dimensional, flexible nanoscale field-effect transistors as localized bioprobes. *Science* **329**, 830–834 (2010).
19. Nikolenko, V., Poskanzer, K. E. & Yuste, R. Two-photon photostimulation and imaging of neural circuits. *Nature Methods* **4**, 943–950 (2007).
20. Peterka, D. S., Takahashi, H. & Yuste, R. Imaging voltage in neurons. *Neuron* **69**, 9–21 (2011).
21. Zhang, F. *et al.* Optogenetic interrogation of neural circuits: technology for probing mammalian brain structures. *Nature Protoc.* **5**, 439–456 (2010).
22. Shalek, A. K. *et al.* Vertical silicon nanowires as a universal platform for delivering biomolecules into living cells. *Proc. Natl Acad. Sci. USA* **107**, 1870–1875 (2010).
23. Thomas, P. & Smart, T. G. HEK293 cell line: a vehicle for the expression of recombinant proteins. *J. Pharmacol. Toxicol. Methods* **51**, 187–200 (2005).
24. Rols, M. P. & Teissie, J. Electropermeabilization of mammalian cells. Quantitative analysis of the phenomenon. *Biophys. J.* **58**, 1089–1098 (1990).
25. Moulton, S. E. *et al.* Studies of double layer capacitance and electron transfer at a gold electrode exposed to protein solutions. *Electrochim. Acta* **49**, 4223–4230 (2004).
26. Dichter, M. A. Rat cortical neurons in cell culture: culture methods, cell morphology, electrophysiology, and synapse formation. *Brain Res.* **149**, 279–293 (1978).
27. Romijn, H. J., Mud, M. T., Habets, A. M. & Wolters, P. S. A quantitative electron microscopic study on synapse formation in dissociated fetal rat cerebral cortex *in vitro*. *Brain Res.* **227**, 591–605 (1981).
28. Kole, M. H. P. & Stuart, G. J. Is action potential threshold lowest in the axon? *Nature Neurosci.* **11**, 1253–1255 (2008).
29. Dan, Y. & Poo, M-M. Spike timing-dependent plasticity: from synapse to perception. *Physiol. Rev.* **86**, 1033–1048 (2006).
30. Mason, A., Nicoll, A. & Stratford, K. Synaptic transmission between individual pyramidal neurons of the rat visual cortex *in vitro*. *J. Neurosci.* **11**, 72–84 (1991).
31. Nicoletti, M. A. L. Brain-machine interfaces to restore motor function and probe neural circuits. *Nature Rev. Neurosci.* **4**, 417–422 (2003).
32. Arancio, O., Kandel, E. R. & Hawkins, R. D. Activity-dependent long-term enhancement of transmitter release by presynaptic 3',5'-cyclic GMP in cultured hippocampal neurons. *Nature* **376**, 74–80 (1995).

Acknowledgements

The authors thank J. MacArthur, E. Soucy, J. Greenwood, L. DeFeo, N. Sanjana, A. Dibos, G. Lau, B. Ilic, M. Metzler, L. Xie and E. Macomber for scientific discussions and technical assistance. The VNEA fabrication and characterization were performed in part at the Center for Nanoscale Systems at Harvard University. This work was supported by an NIH Pioneer award (5DP1OD003893-03) and an NSF EFRI award (EFRI-0835947).

Author contributions

H.P. and J.T.R. conceived and designed the experiments. J.T.R., M.J., A.K.S. and R.S.G. performed experiments, and M-H.Y. helped with the experimental set-up and initiation of the experiments. J.T.R., M.J. and A.K.S. analysed the data. H.P. supervised the project. J.T.R., M.J., A.K.S. and H.P. wrote the manuscript, and all authors read and discussed it extensively.

Additional information

The authors declare no competing financial interests. Supplementary information accompanies this paper at www.nature.com/naturenanotechnology. Reprints and permission information is available online at <http://www.nature.com/reprints>. Correspondence and requests for materials should be addressed to H.P.